Received: 16 November 2023 | Revised: 13 February 2024 | Accepted: 9 March 2024

DOI: 10.1002/trc2.12470

Alzheimer's & Dementia
Translational Research & Clinical Interventions

RESEARCH ARTICLE

Induction of tauopathy in a mouse model of amyloidosis using intravenous administration of adeno-associated virus vectors expressing human P301L tau

Dylan J. Finneran | **Taylor Desjarlais** | **Alayna Henry** | **Brianna M. Jackman** | **Marcia N. Gordon** | **David Morgan**

Department of Translational Neuroscience and the Alzheimer's Alliance, Michigan State University, Grand Rapids, Michigan, USA

Correspondence
Marcia Gordon, Department of Translational Neuroscience, Michigan State University GRRC, 400 Monroe St NW, Grand Rapids, MI 49503, USA.
Email: mngordon@msu.edu

Abstract

INTRODUCTION: Alzheimer's disease (AD) is a progressive neurodegenerative disease in which extracellular aggregates of the amyloid beta (Aβ) peptide precede widespread intracellular inclusions of the microtubule-associated protein tau. The autosomal dominant form of AD requires mutations that increase production or aggregation of the Aβ peptide. This has led to the hypothesis that amyloid deposition initiates downstream responses that lead to the hyperphosphorylation and aggregation of tau.

METHODS: Here we use a novel approach, somatic gene transfer via intravenous adeno-associated virus (AAV), to further explore the effects of pre-existing amyloid deposits on tauopathy. APP+PS1 mice, which develop amyloid deposits at 3 to 6 months of age, and non-transgenic littermates were injected at 8 months of age intravenously with AAV-PHP.eB encoding P301L human tau. Tissue was collected at 13 months and tauopathy was assessed.

RESULTS: Total human tau expression was observed to be relatively uniform throughout the brain, reflecting the vascular route of AAV administration. Phospho-tau deposition was not equal across brain regions and significantly increased in APP+PS1 mice compared to non-transgenic controls. Interestingly, the rank order of phospho-tau deposition of affected brain regions in both genotypes paralleled the rank order of amyloid plaque deposits in APP+PS1 mice. We also observed significantly increased *MAPT* RNA expression in APP+PS1 mice compared to non-transgenic despite equal AAV transduction efficiency between groups.

DISCUSSION: This model has advantages over prior approaches with widespread uniform human tau expression throughout the brain and the ability to specify the stage of amyloidosis when the tau pathology is initiated. These data add further support to the amyloid cascade hypothesis and suggest RNA metabolism as a potential mechanism for amyloid-induced tauopathy.

KEYWORDS
adeno-associated virus, Alzheimer's disease, amyloid, mouse models, tauopathy

1 | BACKGROUND

Alzheimer's disease (AD) is a progressive neurodegenerative disease in which extracellular aggregates of the amyloid beta (Aβ) peptide precede widespread intracellular inclusions of the microtubule-associated protein tau. Mutations in the amyloid precursor protein (APP), presenilin-1 (PS1), and presenilin-2 that modify Aβ processing cause autosomal dominant AD and, therefore, amyloid plaques are suggested to initiate the disease. The amyloid cascade hypothesis[1] posits that amyloid deposition initiates downstream responses that induce tau hyperphosphorylation and aggregation, which is the proximal cause of neuron loss and cognitive decline in AD. While this hypothesis has recently been lent support by successful human trials of anti-amyloid immunotherapies,[2,3] the mechanism(s) by which amyloid facilitates tauopathy are not fully elucidated.

Animal models have been used to investigate the impacts of amyloid pathology on tau pathology. When transgenic mice that develop amyloid or tau pathology are cross bred, they typically demonstrate that amyloid can enhance tauopathy compared to mice transgenic only for human tau.[4–12] In most of these models, there is a clear temporal pattern of amyloid plaques emerging before tauopathy. In 3xTg mice, in which amyloid pathology precedes tauopathy, treatment with anti-Aβ immunotherapy not only depletes amyloid deposits but also reduces tauopathy.[13] However, temporal causes are difficult to discriminate in transgenic mice because both transgenes typically over-express from the moment of conception.

Seeding experiments have also demonstrated amyloid pathology exacerbates tauopathy. Injection of amyloid fibrils, either recombinant or extracted from brain tissue, into tauopathy mouse models increases tau phosphorylation and NFT formation.[14–16] Conversely, injection of tau seeds into mouse models of amyloid deposition demonstrates a dose effect of amyloid pathology on the magnitude of the resulting tau pathology.[17,18]

Limited work has been done using somatic gene transfer, typically of tau-expressing vectors into models of amyloid deposition. Klein et al.[19] injected AAV2-4N2R tau with the P301L mutation associated with frontotemporal dementia[20] into male Sprague-Dawley rat septum and APP+PS1 transgenic mouse hippocampus. Both rodent species developed tau inclusions in neurons of injected brain regions. In addition, APP+PS1 mice displayed prominent transduced tau expression in dystrophic neurites surrounding amyloid deposits. Dassie et al.[21] stereotaxically injected AAV6 encoding several tau genetic variants or green fluorescent protein (GFP) control into entorhinal cortex of TASTPM (APP/PS1) transgenic mice, non-transgenic mice, or tau knock-out controls. They reported that tau variants caused time-dependent neuron loss in both amyloid mice and non-transgenic mice. No differences in tau pathology were reported in amyloid versus non-transgenic mice. No changes in amyloid burden after AAV-tau administration were observed. Koller et al.[22] used AAV1 to over-express tau genetic variants or GFP (control) in CRND8-APP transgenic mice. They contrasted injections at postnatal day 1 (P1; before amyloid deposition) or at P90 when amyloid deposition has started. Three months of over-expression of mutant tau, but not wild-type tau, induced tau deposition and the formation of Gallyas-positive inclusions in the P90 mice, but not in mice injected at P1. However, in P1 injected mice they detected a large increase in Aβ deposition with mutant tau at the 3-month survival time. Quantitation of soluble total tau pools by western blot was performed to compare the different viral constructs in APP mice, but comparisons to non-transgenic mice were not presented.

Intracranial administration of viral vectors can result in large over-expression of genes of interest. However, single injections have a limited distribution area as well as a gradient of expression from the site of delivery. It is now possible to deliver genes across the blood-brain barrier using specific capsid modifications to allow widespread expression across the brain.[23,24] Consequently, we used this approach to deliver adeno-associated virus (AAV) expressing human 4R2N tau with the P301L mutation into non-transgenic (NonTg) or APP+PS1 mice in middle age, at which point APP+PS1 mice have accumulated significant amyloid pathology. This timepoint was chosen to better reflect the natural disease progression in AD patients with mature amyloid pathology preceding by up to a decade the emergence of tau pathology. We achieved expression of human *MAPT* approximately equivalent to that of endogenous mouse *Mapt* and examine effects of pre-existing amyloid on tau phosphorylation and aggregation. The expression was relatively uniform throughout the brain and we noted considerable increases in tauopathy in APP+PS1 mice with existing amyloid deposits versus non-transgenic littermates of the same age.

2 | METHODS

2.1 | Animals

APP+PS1 mice were originally generated by crossing Tg2576 mice, carrying mutated human APP (K595N/M596L), and PS1 line 5.2, carrying mutated PS1 (M146L).[25] The transgenes segregate independently. This colony has been maintained as a closed-outbred colony since 1998. Genotype of experimental mice was determined from ear punch biopsy at weaning and confirmed after euthanasia by Transnetyx, Inc. The light cycle was maintained at 12-hour light/12-hour dark. Although excessive aggression in APP+PS1 male mice often requires single housing, mice were group housed until enrollment into the experiment, when possible. All mice were singly housed prior to viral

vector injection. The mice were given food and water ad libitum. Each treatment condition consisted of ≈ 50% male and 50% female mice.

2.2 | Cloning and adeno-associated virus production

Human tau (4R2N) with the P301L mutation was cloned into the pTR MCSW at the AgeI and NheI restriction sites. Resulting clones were restriction digested to confirm presence of inverted terminal repeats and sequenced. The vector, pTR P301L-W, contained AAV2 terminal repeats, the ubiquitous CAG promoter, human P301L tau, the woodchuck hepatitis virus posttranscriptional regulatory element, and the bovine growth hormone poly-A signal for transcription termination. Expression of this vector was confirmed by transfection into 293T cells. The construct encoding PHP.eB (pUCmini-iCAP-PHP.eB) was a generous gift from Viviana Gradinaru (Addgene plasmid # 103005;RRID:Addgene_103005; http://n2t.net/addgene:103005). [23] Recombinant AAV-PHP.eB particles were generated using the triple transfection method as described previously[26] and quantified using the dot-blot method with a non-radioactive biotinylated probe for human tau generated by polymerase chain reaction (PCR).

2.3 | AAV injection and tissue collection

Eight-month-old APP+PS1 ($n = 20$, 9 female and 11 male) and NonTg ($n = 14$, 7 female and 7 male) littermates were injected with 100 μL of 4.8×10^{13} vg/mL PHP.eB-P301L-W tau in the lateral tail vein. Eleven of the APP+PS1 mice (5 female and 6 male) also received a control dendritic cell (DC) vaccine comprised of 1.2×10^{6} unstimulated murine dendritic cells in 0.25 mL saline administered as an intraperitoneal injection 4, 6, and 8 weeks after AAV administration. The measures of tauopathy in the control vaccine mice and untreated APP+PS1 mice ($n = 9$, 4 female and 5 male) were identical for all measures except insoluble pS199 tau in the hippocampus (Figure S4 in supporting information). See supplemental figures in supporting information for complete analysis and comparison of these two groups. We combined these two groups for all other tau measures in the analysis but indicate the DC injected mice with open symbols in the figures presented here. Five months after AAV injection, mice were weighed and injected with a solution containing pentobarbital (100 mg/kg) and phenytoin (12.5 mg/kg). The deeply anesthetized mice were transcardially perfused with 25 mL of 0.9% saline. Right hemibrain was dissected into anterior cortex, posterior cortex, hippocampus, and cerebellum which were snap frozen on dry ice. Left hemibrain was fixed in 4% paraformaldehyde for 24 hours at 4°C. The fixed hemisphere was cryoprotected in sucrose by successive 24-hour incubations in 10%, 20%, and 30% sucrose. Brains were frozen on a cold stage and sectioned horizontally into 25 μm thick sections with a sliding microtome. Sections were stored in phosphate-buffered saline (PBS) with 10 mM sodium azide at 4°C.

Research in Context

Systematic Review: The authors studied the literature available in PubMed on mouse models of amyloid-induced tauopathy. We found several reports on transgenic mice with both amyloid and tau pathology but none using somatic gene transfer to model Alzheimer's-like pathology.

Interpretation: Our findings are consistent with the amyloid cascade hypothesis and our model has advantages over other approaches. Furthermore, our data hint at a potential mechanism for amyloid-induced tauopathy in Alzheimer's disease.

Future Directions: This article describes a new mouse model of amyloid-induced tauopathy. We believe this model has advantages over transgenic mice and can be used to explore potential mechanisms of amyloid-induced tauopathy. For instance, future studies may examine the role of innate immune activity or severity of existing amyloidosis on exacerbating tauopathy.

2.4 | Tissue homogenization and enzyme-linked immunosorbent assay

Frozen brain regions were weighed and homogenized in radioimmunoprecipitation assay buffer (RI10 μL per mg wet tissue mass) with protease inhibitor cocktail (Sigma Aldrich, Cat. No. P8340), deacetylase inhibitor cocktail (Med Chem Express, Cat. No. HY-K0030), and phosphatase inhibitor cocktails II and III (Sigma Aldrich, Cat. Nos. P5726 and P0044, respectively). The homogenate was sonicated (three 3-second pulses, 40% amplitude) and centrifuged at 50,000 x g for 1 hour at 4°C. The resulting supernatant was transferred to a new tube, assayed for total protein by Pierce bicinchoninic acid (BCA; ThermoFisher, Cat. No. 23227), and frozen. The pellet was sonicated (three 3-second pulses) and digested in 70% formic acid (2 μL per mg wet tissue mass) for 1 hour at room temperature and then neutralized in 167 mM Tris, assayed for total protein by BCA, and frozen. Invitrogen enzyme-linked immunosorbent assay (ELISA) kits were used to analyze human total tau (ThermoFisher, Cat. No. KHB0041), pSer396 phospho-tau (ThermoFisher, Cat. No. KHB7031), pSer199 phospho-tau (ThermoFisher, Cat. No. KHB7041), Aβ 42 (ThermoFisher, Cat. No. KHB3441), Aβ 40 (ThermoFisher, Cat. No. KHB3481), and Aβ aggregate (ThermoFisher, Cat. No. KHB3491). Prior to ELISA analysis, supernatant and formic acid samples were diluted in 1X PBS and sample buffer to be within standard curve range of each respective ELISA. Kits were performed per manufacturer's instructions.

2.5 | Nucleic acid isolation and quantitative PCR

Genomic DNA and RNA were isolated simultaneously from posterior cortex using Qiagen's "AllPrep" Kit per the manufacturer's instructions.

RNA and gDNA were quantified by nanodrop. RNA was reverse transcribed to cDNA using Bio-Rad iScript RT and the relative expression of human tau (*MAPT*) and mouse tau (*Mapt*) RNA was determined by quantitative PCR (qPCR) using the relative standard curve method. The housekeeping gene *Gapdh* was used as a loading control. The gDNA fraction was assayed for AAV genomes using the primer/probe set specific for *MAPT* and normalized to *Gapdh*. Primer/probe sets were from ThermoFisher: *MAPT* assay number Hs00213941_m1, *Mapt* assay number Mm00521988_m1, *Gapdh* assay number Mm99999915_g1.

2.6 | Immunohistochemistry

Six to eight evenly spaced horizontal sections spanning the brain were chosen for analysis. Immunohistochemistry experiments were performed as described previously.[27] Commercially available antibodies were purchased with biotin conjugation from ThermoFisher (HT7 Cat. No. MN1000B; AT8 Cat. No. MN1020B). The mouse monoclonal antibody PHF-1 was a kind gift from Peter Davies. It was first purified from cell culture supernatant using a kit following the manufacturer's instructions (Abcam Cat. No. ab128745). After purification, it was biotinylated using a kit following the manufacturer's instructions (Abcam Cat. No. ab201795). For Congo red, sections were mounted onto slides first and allowed to dry. Slides were stained for Congo red using a kit per the manufacturer's instructions (Abcam). For immunostaining, floating sections for each animal were placed into a multi-sample staining tray. Endogenous peroxidases were blocked (10% methanol, 3% hydrogen peroxide in PBS) and tissue was permeabilized (0.2% lysine, 0.1% Triton X-100, 4% goat serum in PBS). Sections were incubated at room temperature overnight in the appropriate primary antibody in 4% goat serum in PBS. Sections were washed three times in PBS and incubated for 2 hours at room temperature with biotinylated secondary antibody in 4% goat serum in PBS if necessary. After three PBS washes, the sections were incubated with Vectastain Elite ABC kit for enzyme conjugation for 1 hour at room temperature. Sections were stained with 0.05% diaminobenzidine with nickel enhancement and 0.03% hydrogen peroxide for 5 minutes at room temperature. Each assay omitted some sections from primary antibody incubation to evaluate non-specific binding of the secondary antibody. Sections were mounted onto slides, dehydrated, and cover slipped. Slides were digitized using the Zeiss AxioScan.Z1 scanning microscope. Neurocyte IAE software (created by Andrew Lesniak) used hue, saturation, and intensity (I) to segment the images and identify threshold settings using the lightest and darkest sections. Once identified, these values were held constant for analysis of every section labeled with that stain. The percent area staining was determined mathematically by dividing the number of segmented pixels by the total number of pixels in the region of interest.

2.7 | Statistical analysis

Statistical analysis was performed using GraphPad Prism Statistics Software version 9.5.0. Mann–Whitney *U* test was performed to compare NonTg mice to APP+PS1 mice. A one-way analysis of variance was used to examine regional differences in tau expression within genotypes. Linear regression analysis was used to examine a correlation between AT8 phospho-tau and Congophilic plaques as well as transduction efficiency and anterior cortical tau ELISA values.

3 | RESULTS

3.1 | Increased tau phosphorylation in APP+PS1 mice

To assess tau pathology, both soluble and insoluble brain fractions were assayed for total tau, pSer199 phospho-tau, and pSer396 phospho-tau by ELISA. Mouse genotype was associated with pronounced changes in tauopathy in the anterior cortical region. The presence of amyloid deposits in APP+PS1 mice increased soluble and insoluble total tau (Figure 1A and B), soluble and insoluble pSer199 phospho-tau (Figure 1C and D), as well as soluble and insoluble pSer396 phospho-tau (Figure 1E and F). In the hippocampus, APP+PS1 mice had a significant increase in soluble total tau and pSer199 phospho-tau compared to NonTg mice (Figure 2A and C) but not the PHF-associated phosphorylation site, pSer396 phospho-tau. None of the insoluble tau species measured were significantly elevated in the hippocampus of APP+PS1 mice by ELISA (Figure 2B, D–F).

Tau pathology was also measured histologically using the anti-human total tau antibody HT7, the anti-phospho-tau antibody AT8 (pS202/pT205, an early tauopathy marker), and the anti-human phospho-tau antibody PHF-1 (pS396, a paired helical filament-associated marker). In both APP+PS1 and NonTg mice, there was widespread expression of total tau in most brain regions, with more expression in gray matter than white matter, but no regional hot spots or steep gradients of expression as found with intracranial injections of AAV vectors (Figure 3A and 3B). Furthermore, there was strong staining of neurons in both the cortex (Figure 3C, D) and the hippocampus (Figure 3E, F). Although not quantified, this neuronal staining is consistent with the 25% to 30% of neurons labeled by GFP in our prior work.[24]

AT8 staining overall was less intense than the total tau staining, and less uniform with little staining in striatum or thalamus, and concentrated staining in cortical regions (Figure 3G and H). The percentage of cortical neurons labeled by AT8 appeared less than HT7, and this was particularly true for the NonTg mice (compare Figure 3D to 3J). In the hippocampus, AT8 staining was largely restricted to neuritic deposits in the vicinity of amyloid plaques in APP+PS1 mice, rather than staining entire neurons (Figure 3K). Non-transgenic mice display no amyloid deposits and minimal levels of AT8 staining (Figure 3L). Very limited and light staining for another phospho-tau antibody, PHF-1, was observed in both APP+PS1 and NonTg mice. Staining was largely restricted to the anterior cortex. Using a rubric to score the intensity and distribution of staining, we observed significantly more PHF-1 staining in APP+PS1 mice than NonTg mice (Figure S9 in supporting information). The limited PHF-1 positivity indicates the tauopathy has not fully matured to the paired helical filament stage.

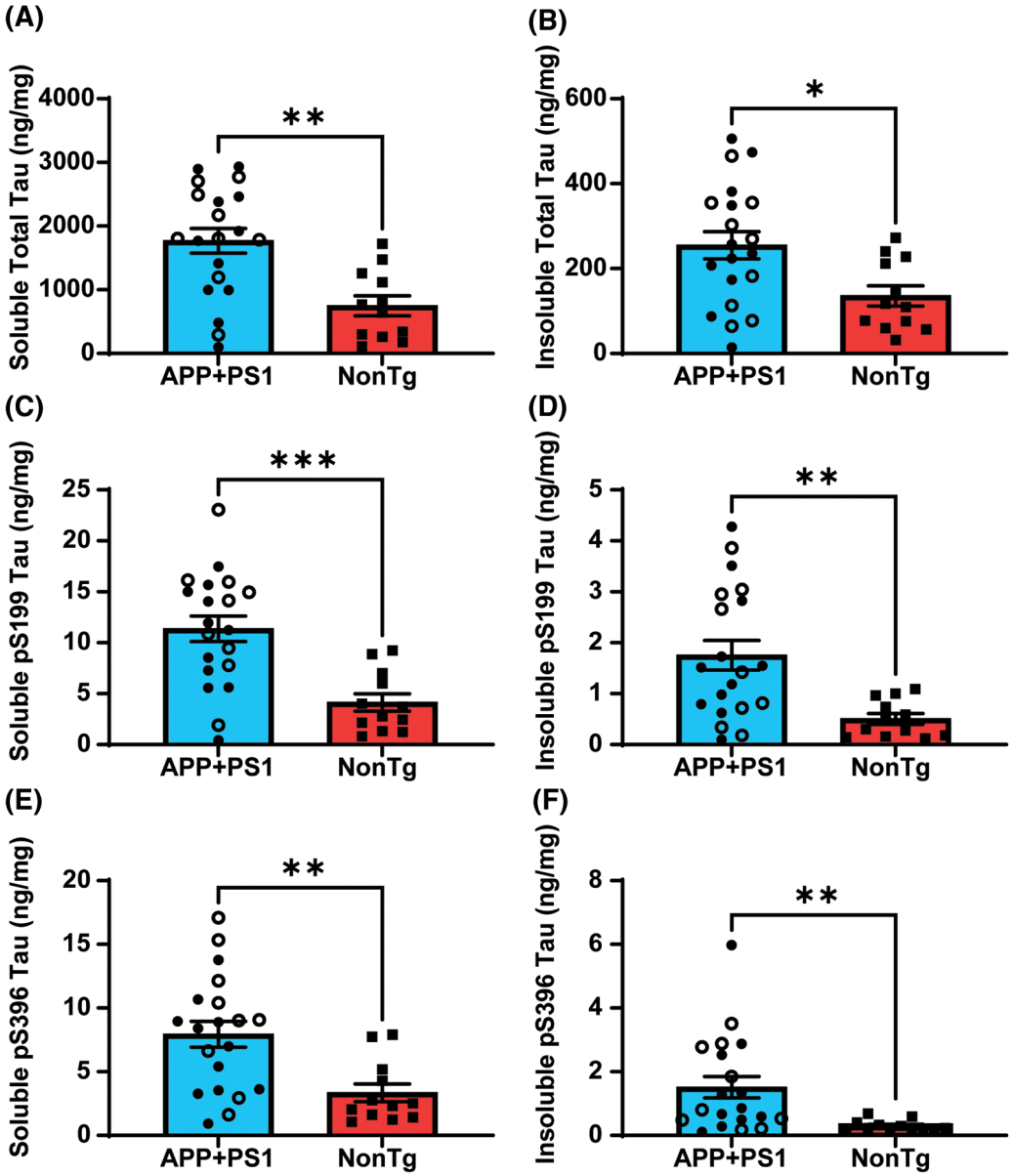

FIGURE 1 Increased tauopathy in anterior cortex of APP+PS1 mice.
Graph of RIPA-soluble (A) and RIPA-insoluble (B) total tau. Graph of RIPA-soluble (C) and RIPA-insoluble (D) pSer199 phospho-tau. Graph of RIPA-soluble (E) and RIPA-insoluble (F) pSer396 phospho-tau. There was a significant increase in all tau markers, both soluble and insoluble, in APP+PS1 mice. Open circles are APP+PS1 mice that received no vaccine. Filled circles are APP+PS1 mice that received control vaccine. Data are presented as mean ± standard error of the mean, $n = 12–20$. $^{*}P < 0.05$, $^{**}P < 0.01$, and $^{***}P < 0.001$ by Mann–Whitney test. APP, amyloid precursor protein; NonTg, non-transgenic; PS1, presenilin-1; RIPA, radioimmunoprecipitation assay buffer.

We quantified immunostaining of AT8 in four brain regions: anterior cortex, posterior cortex, hippocampus, and striatum. In every brain region, there was a larger amount of staining in the APP+PS1 mice than the NonTg mice that ranged from 2.5- to 6-fold (Figure 4). Interestingly, although amounts were quite low, there was increased total and phospho-tau in the striatum, a brain region we have previously demonstrated has diffuse, but not Congophilic, amyloid plaques in this amyloidosis model.[27]

3.2 | Presence of amyloid accelerates development of tauopathy

Next, we examined the relative vulnerability of different brain regions to the development of tauopathy. While there was no significant difference in total tau expression among brain regions in APP+PS1 (Figure 5A) or NonTg mice (Figure 5C), there was a significant difference in the percent area staining of AT8 phospho-tau in the APP+PS1

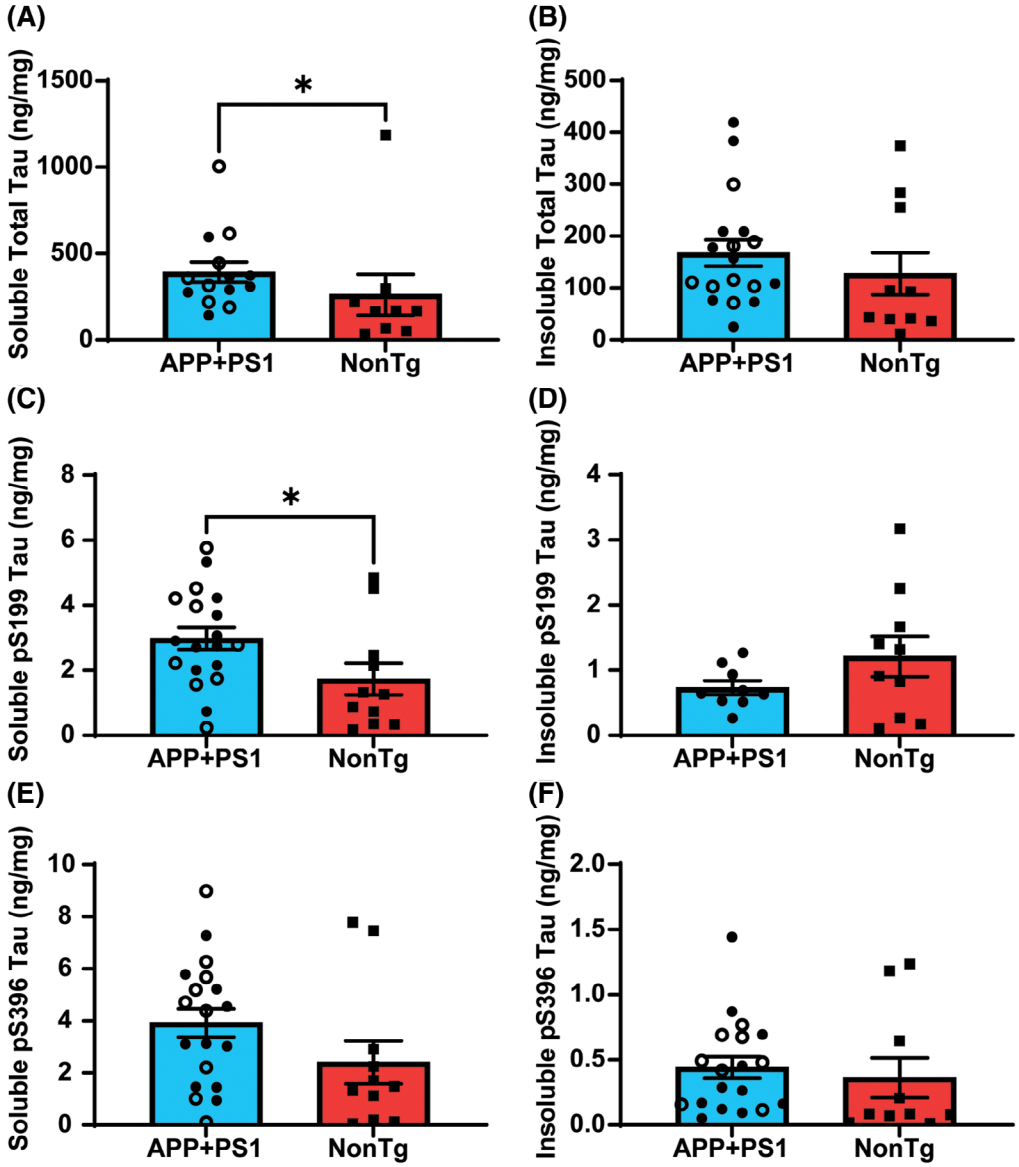

FIGURE 2 Modest increase in total soluble and pS199 tau in the hippocampus of APP+PS1 mice. Graph of RIPA-soluble (A) and RIPA-insoluble (B) total tau. There was significantly more insoluble total tau in APP+PS1 mice compared to NonTg mice. Graph of RIPA-soluble (C) and RIPA-insoluble (D) pSer199 phospho-tau. Graph of RIPA-soluble (E) and RIPA-insoluble (F) pSer396 phospho-tau. Open circles are APP+PS1 mice that received no vaccine. Filled circles are APP+PS1 mice that received control vaccine. Data are presented as mean ± standard error of the mean, $n = 9–20$. *$P < 0.05$ by Mann–Whitney test. APP, amyloid precursor protein; NonTg, non-transgenic; PS1, presenilin-1; RIPA, radioimmunoprecipitation assay buffer.

mice (one-way analysis of variance [ANOVA] F[3, 75] = 24.01, $P < 0.0001$; Figure 5B) and in the NonTg mice (one-way ANOVA F[3, 45] = 7.210, $P = 0.0005$; Figure 5D). The rank order of the brain regions was the same in both genotypes with anterior cortex > posterior cortex > hippocampus > striatum. A similar regional rank order of Congophilic plaque load in APP+PS1 mice was observed (with anterior cortex > posterior cortex = hippocampus > striatum Figure 5E). Linear regression of the mean values of AT8 staining and Congo red staining for the APP+PS1 mice indicated a significant positive correlation of amyloid burden with AT8 immunostaining (Figure 5F).

3.3 | Increased *MAPT*, but not transduction efficiency, in APP+PS1 mice

To rule out genotype effects on viral transduction efficiency as an explanation for the observed differences in tauopathy, we performed qPCR for the AAV genome on genomic DNA isolated from posterior cortex. We compared PCR for both human *MAPT* DNA and murine *Mapt* DNA. There was no significant difference in viral genomes per mouse genome in APP+PS1 mice compared to NonTg mice (Figure 6A). We also note that the mean value equaled 1, indicating there was an

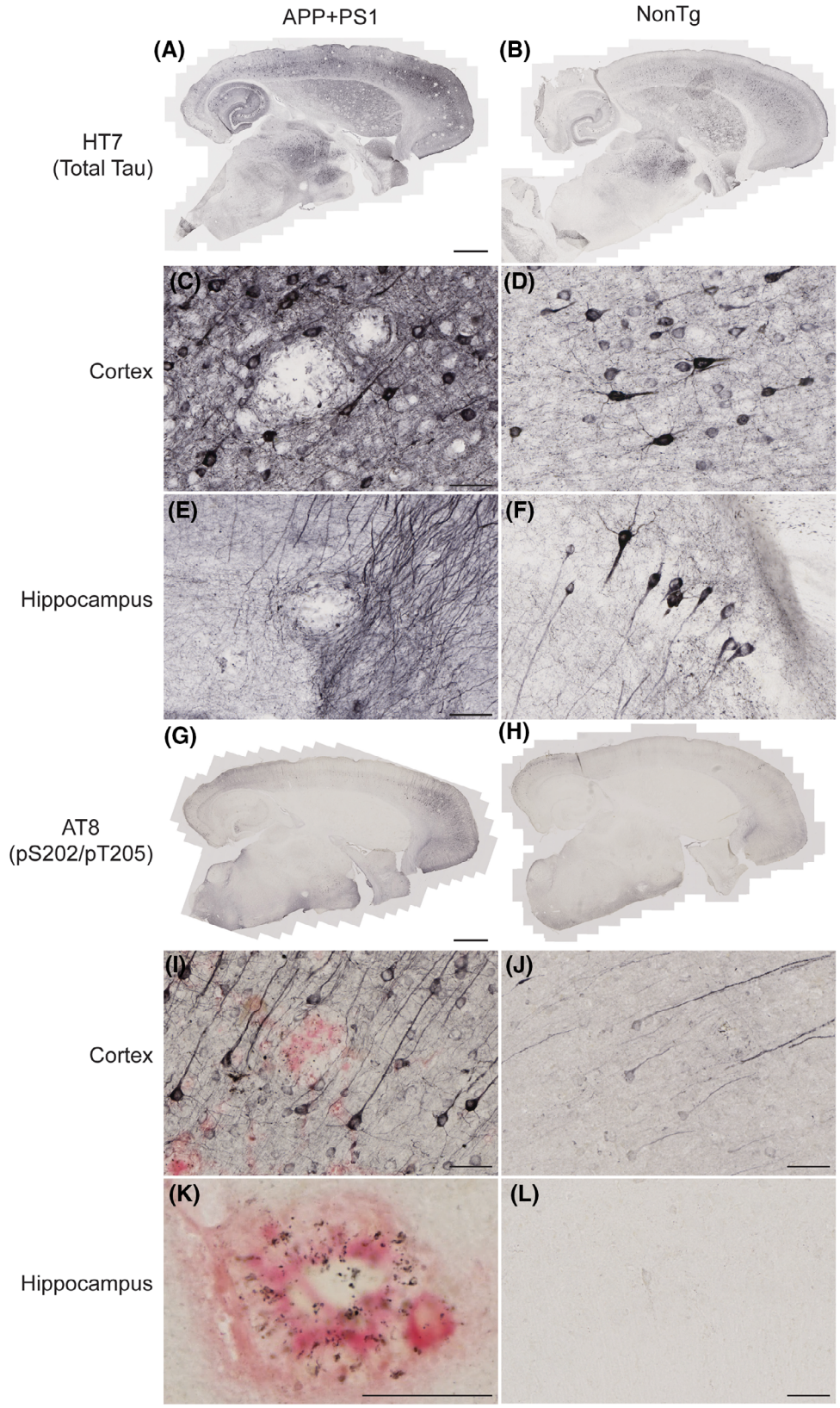

FIGURE 3 Tau immunostaining in APP+PS1 and NonTg mice. A–F, Representative images of total tau staining in APP+PS1 (left column) and NonTg mice (right column). APP+PS1 mice show greater area staining than NonTg mice but similar brain-wide distribution of tau expression. Prominent staining of neuronal profiles is observed in both cortex (C, D) and hippocampus (E, F). G–L, Representative images of phospho-tau staining in APP+PS1 and NonTg mice with Congo red counter-stain, revealing regional variation in staining. In cortex, phospho-tau staining is largely restricted to neuronal profiles in the brains of both APP+PS1 (I) and NonTg mice (J). In APP+PS1 mice, hippocampal AT8 staining is prominent in dystrophic neurites surrounding Congophilic plaques (K). Non-transgenic mice display no amyloid deposits and little phospho-tau staining (L). Scale bar = 1000 μm (A, B, G, H) or 50 μm (C–F, J–L). APP, amyloid precursor protein; NonTg, non-transgenic; PS1, presenilin-1.

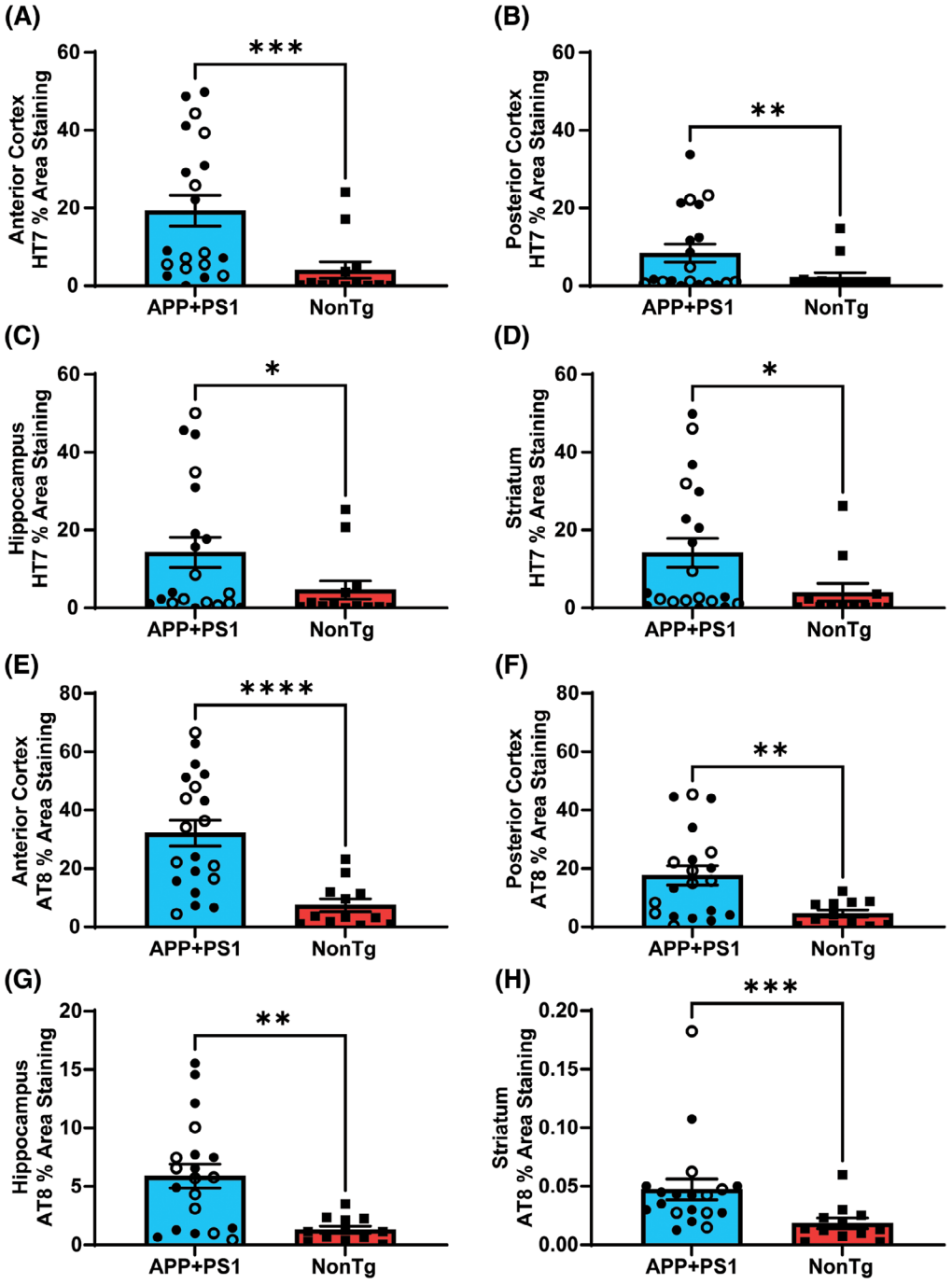

FIGURE 4 Increased tau immunostaining in APP+PS1 mice. Graph of percent area staining of total tau (HT7) in the anterior cortex (A), posterior cortex (B), hippocampus (C), and striatum (D). APP+PS1 mice (blue columns) had significantly greater percent area staining of HT7 tau than NonTg mice (red columns) in each brain region measured. Graph of percent area staining of phospho-tau (AT8) in the anterior cortex (E), posterior cortex (F), hippocampus (G), and striatum (H). APP+PS1 mice (blue columns) had significantly greater percent area staining of AT8 tau than NonTg mice (red columns) in each brain region measured. Open circles are APP+PS1 mice that received no vaccine. Filled circles are APP+PS1 mice that received control vaccine. Data are presented as mean ± standard error of the mean, $n = 12–20$. $^{*}P < 0.05$, $^{**}P < 0.01$, $^{***}P < 0.001$, and $^{****}P < 0.0001$ by Mann–Whitney test. APP, amyloid precursor protein; NonTg, non-transgenic; PS1, presenilin-1.

overall doubling of tau DNA caused by the viral transduction. We then performed real-time PCR on the human *MAPT* RNA fraction obtained from the posterior cortex. We did observe significantly greater *MAPT* mRNA in APP+PS1 mice relative to NonTg mice of approximately 2-fold (Figure 6B). Of note, this method of systemic administration of AAV with the PhP.eB capsid produced a physiological, modest (≈ 50%) over-expression of exogenous *MAPT* in APP+PS1 mice compared to endogenous *Mapt*.

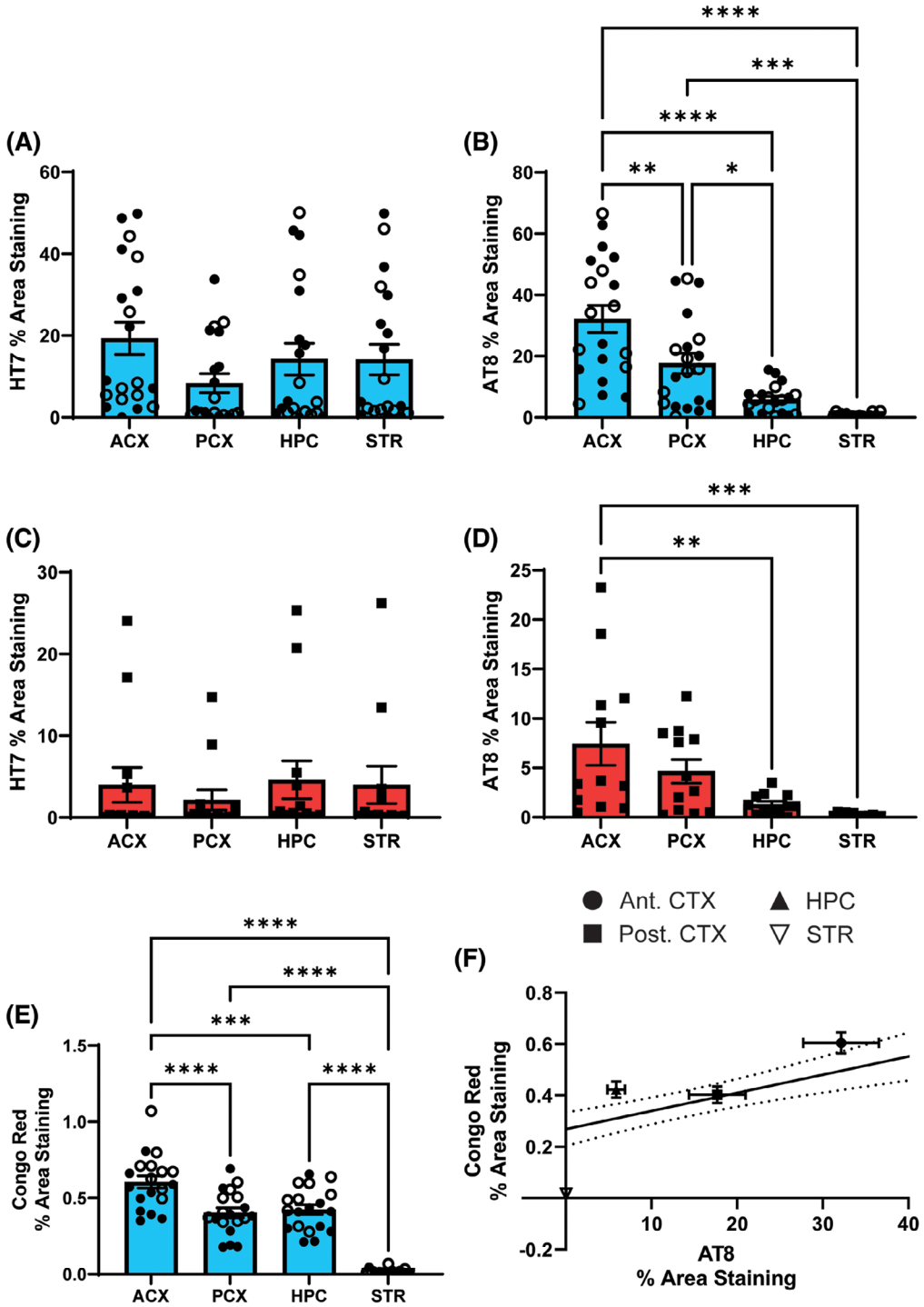

FIGURE 5 Tauopathy correlates with Congophilic plaque burden in different brain regions. A, Graph of percent area staining of human total tau (HT7) in APP+PS1 mice. B, Graph of percent area staining of AT8 phospho-tau in APP+PS1 mice. C, Graph of percent area staining of total tau in non-transgenic mice. D, Graph of percent area staining of AT8 phospho-tau in non-transgenic mice. There was no significant difference in total tau area staining between brain regions in either APP+PS1 or NonTg mice. However, significantly more AT8 area staining was observed in cortical regions of APP+PS1 and NonTg mice. E, Percent area staining of Congo red in APP+PS1 mice revealed similar regional differences in staining. F, Graph of percent area AT8 staining versus percent area Congo red staining in the different brain regions of APP+PS1 mice. There was a significant correlation (Spearman $r = 0.6577$, $P < 0.0001$). Dashed lines represent 95% confidence interval for best-fit line. Open circles are APP+PS1 mice that received no vaccine. Filled circles are APP+PS1 mice that received control vaccine. Data are presented as mean ± standard error of the mean, $n = 12–20$. $^{*}P < 0.05$, $^{**}P < 0.01$, $^{***}P < 0.001$, $^{****}P < 0.0001$ by one-way analysis of variance and Tukey post hoc tests. ACX, anterior cortex; APP, amyloid precursor protein; HPC, hippocampus; NonTg, non-transgenic; PCX, posterior cortex; PS1, presenilin-1; STR, striatum.

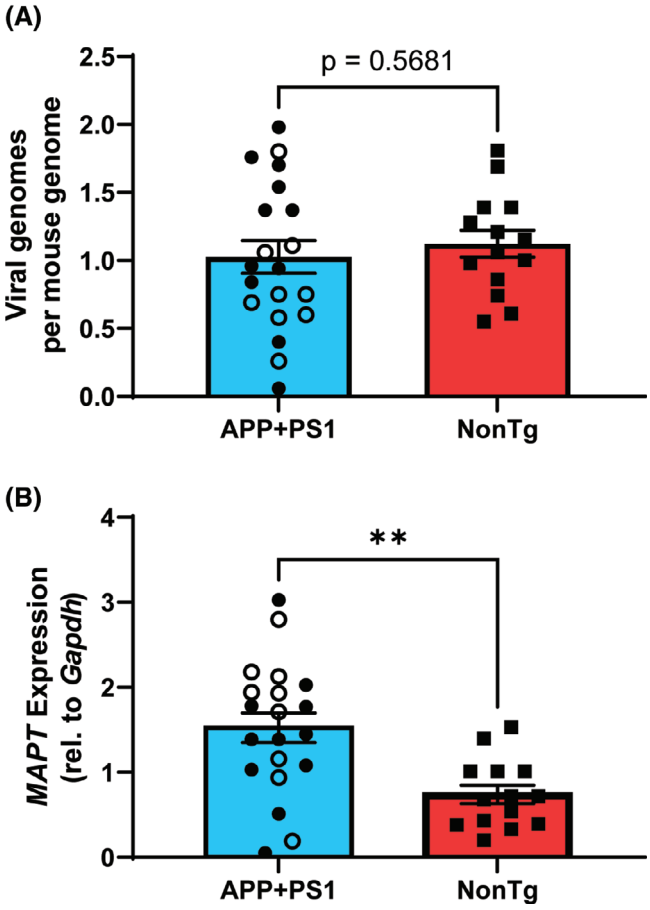

FIGURE 6 Equivalent transduction but increased *MAPT* expression in APP+PS1 mice. A, Graph of viral genomes relative to mouse genomes measured by quantitative polymerase chain reaction. B, Graph of *MAPT* expression relative to *Gapdh* expression. No significant difference in viral genomes per mouse genome was observed, but there was a significant increase in *MAPT* expression in APP+PS1 (blue columns) compared to NonTg mice (red columns). Open circles are APP+PS1 mice that received no vaccine. Filled circles are APP+PS1 mice that received control vaccine. Data are presented as mean ± standard error of the mean, $n = 12–20$. $^{**}P < 0.01$ Mann–Whitney test. APP, amyloid precursor protein; NonTg, non-transgenic; PS1, presenilin-1.

3.4 | Tau ELISA measures correlate with transduction efficiency

We correlated the number of viral genomes per mouse with the ELISA levels for soluble and insoluble tau values obtained by ELISA in the anterior cortex. Table 1 shows the correlation coefficients and *P* values for these regressions. Most are statistically significant, indicating that much of the variance in tau levels was secondary to differences in viral transduction efficiency, especially in NonTg mice. However, for a given quantity of viral genomes, tau levels are enhanced in the APP+PS1 mice relative to the NonTg mice, evidenced by the upward shift of the regression line (Figure 7). In addition, transduction efficiency explains less of the variance in the tau measures in the APP+PS1 mice than NonTg mice, probably because of additional variance caused by degree of amyloidosis. Furthermore, the NonTg mice with the highest transduction efficiency still have lower tau levels than APP+PS1 mice with less transduction efficiency.

TABLE 1 Correlation between number of viral genomes (transduction efficiency) and enzyme-linked immunosorbent assay measures of tau and phosphorylated tau.

	APP+PS1	NonTg
ACX S1 Total Tau	Spearman $r = 0.63$	Spearman $r = 0.92$
	$P = 0.003$	$P < 0.0001$
ACX FA Total Tau	Spearman $r = 0.76$	Spearman $r = 0.87$
	$P < 0.0001$	$P = 0.0005$
ACX S1 pS199 Tau	Spearman $r = 0.54$	Spearman $r = 0.88$
	$P = 0.014$	$P = 0.0003$
ACX FA pS199 Tau	Spearman $r = 0.69$	Spearman $r = 0.88$
	$P = 0.0008$	$P = 0.0003$
ACX S1 pS396 Tau	Spearman $r = 0.43$	Spearman $r = 0.87$
	$P = 0.06$	$P = 0.0005$
ACX FA pS396 Tau	Spearman $r = 0.67$	Spearman $r = 0.86$
	$P = 0.0013$	$P = 0.0006$

Abbreviations: ACX, anterior cerebral cortex; FA, detergent insoluble, formic acid soluble fraction; S1, soluble fraction.

4 | DISCUSSION

The primary outcome of this work is additional support for the amyloid cascade hypothesis[1] that Aβ deposits can accelerate the development of tauopathy. While certainly consistent with the prior work using transgenic crosses and intracranial administration of proteins cited in the introduction, the findings here appear to be the first head-to-head comparison using a gene therapy approach. The three prior publications injecting AAV-tau constructs into APP mouse models of amyloidosis did not directly compare tauopathy results to a parallel group of mice lacking amyloid.[19,21,22] A second novel outcome in this study was measurement of an increase in tau RNA expression in the amyloid mice compared to mice lacking amyloid, despite similar levels of transduction assessed by viral DNA content. We are unaware of other studies of amyloid-induced tauopathy that have performed this measurement. While the suggestion that this is part of the mechanism by which amyloid enhances tauopathy development is speculative, we look forward to tests of this possibility in future studies.

A third outcome was the regional differences in both the levels of pathological amyloid and pathological tau. There was a strong regional correlation between the Congo red positive, compacted amyloid deposits and the AT8 marker of early-stage pre-tangle tau pathology. One explanation would be that the compacted plaques modify the local environment to promote development of tauopathy. However, the same regional rank order of AT8 tau pathology, even at low levels, in NonTg mice implies that there is some other regional characteristic that is modifying the degree to which both amyloid pathology and

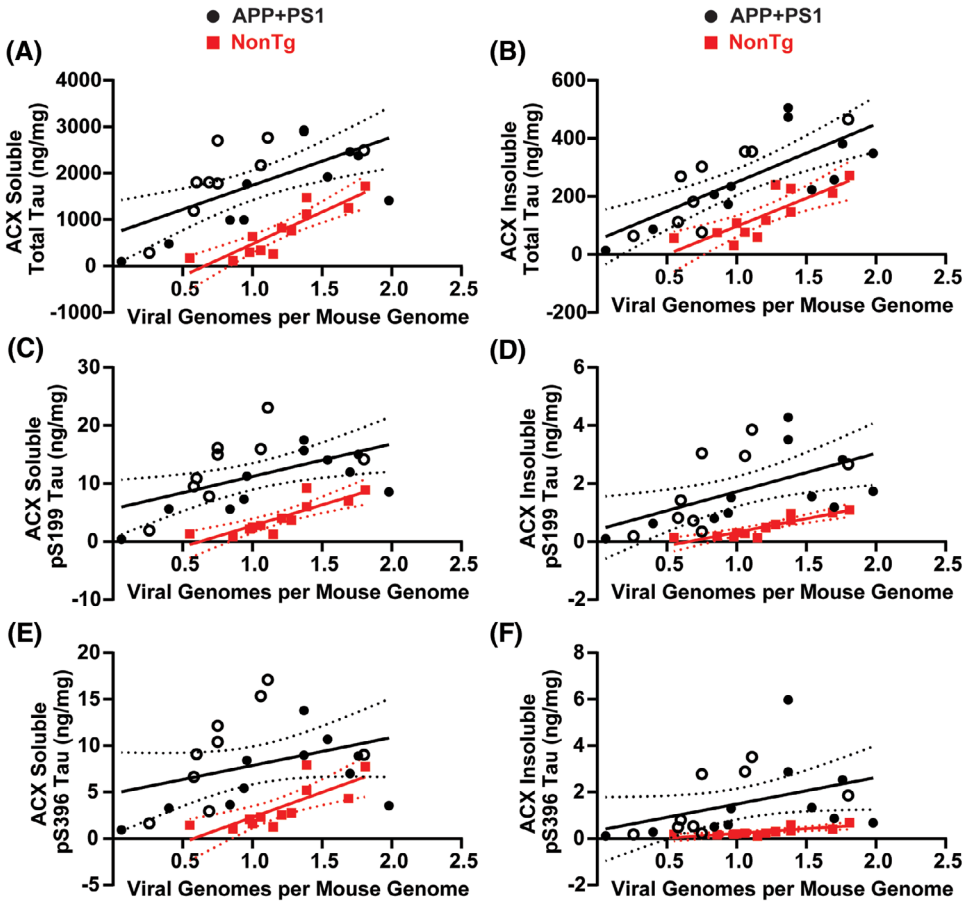

FIGURE 7 Cortical tau ELISA values correlate with transduction efficiency. Graph of linear correlation of viral genomes per mouse genome versus soluble (A) or insoluble (B) total tau ELISA values in the anterior cortex. C, Graph of linear correlation of viral genomes per mouse genome versus soluble or insoluble (D) pS199 tau ELISA values in the anterior cortex. E, Graph of linear correlation of viral genomes per mouse genome and soluble pS396 tau ELISA values in the anterior cortex. The correlation in APP+PS1 mice is not significant for this measure. F, Graph of linear correlation of viral genomes per mouse genome and insoluble pS396 tau ELISA values in the anterior cortex. For each marker, the upward shift in the correlations reveal increased tauopathy in APP+PS1 mice. APP+PS1 mice and best-fit line plotted in black. Open circles are APP+PS1 mice that received no vaccine. Filled circles are APP+PS1 mice that received control vaccine. NonTg mice and best-fit line plotted in red. Dashed lines represent 95% confidence intervals. Correlation was performed using two-tailed non-parametric Spearman correlation, $n = 12–20$. APP, amyloid precursor protein; ACX, anterior cortex; ELISA, enzyme-linked immunosorbent assay; NonTg, non-transgenic; PS1, presenilin-1.

tau pathology accumulate. This is consistent with the work of Paulson et al.[28] who developed a mouse expressing both mutant APP and mutant tau driven by the same Ca^{2+}/calmodulin-dependent protein kinase II (Camk2) promoter system, in which deposition in the cortex preceded the hippocampus and other brain regions. Our own early work with the APP+PS1 mouse model confirms the earlier and greater accumulation of Aβ in the anterior cortex than in the hippocampus (or striatum).[27] This rank order is consistent with the Thal staging in *post mortem* human brains as well.[29] Understanding the molecular differences among these regions might provide insight into features that enhance development of AD pathology in general.

This systemic gene therapy approach has several advantages over intracranial administration approaches. First, it avoids the need for a craniotomy and introduction of injection needles into the brain, which cause damage to tissues that, even if minor, can influence outcomes. Second, it produces a relatively uniform distribution of the viral vector throughout the brain. Both intraparenchymal and intraventricular administrations produce regional gradients of transduction and none can transduce all portions of the brain.[30,31] In this study, we also achieved the desired effects with low levels of transgene over-expression, approximating endogenous expression. Third, compared to most transgenic cross models, this approach permits specifying when the initiation of tauopathy starts relative to the extent of amyloidosis. In this study, we opted to initiate transgene over-expression after widespread and prolonged amyloid deposition to mimic the disease progression more closely to that of AD patients. Future studies can be designed to determine what role aging may play on the emergence of tauopathy. One of the few transgenic mouse studies which failed to see enhanced tauopathy when crossed with an amyloid mouse used the J 20 line crossed with the Tg4510.[32] The first histological tau deposits in Tg4510 begin at 3 to 4 months while the first amyloid deposits in J20 occur several months later. Thus, the tauopathy was mature before the amyloidosis became present, possibly precluding the induction. Another advantage relative to transgenic cross approaches is that it

avoids any developmental effects of the tau transgene. Recently, this same advantage of specifying the time of induction was achieved in a transgenic cross approach with an APP/PS1 mouse crossed with a regulatable tau mouse (Tg4510), in which the tau expression was repressed by doxycycline.[33] They maintained the repression for 15 months and then removed doxycycline for 6 months. The Tg4510 mice on the amyloid background developed tauopathy but the mice on the standard Tg4510 background failed to deposit over the same time frame. The one limitation to this approach is the extensive breeding to achieve mice with the three required transgenes.

There are some disadvantages to this systemic gene therapy approach. One is that roughly one third of neurons are transduced with AAV-PHP.eB. For manipulations that require most targeted cells to carry the therapeutic gene, this would be a limitation. A second disadvantage is possible effects on peripheral organs. Expression of tau in other organs might produce complications that could interfere with data interpretation. Although this can be diminished by selection of neuron-specific promoters,[24] other cells would still be transduced with AAV. Another limitation is that not all mouse lines express the receptor variant responsible for the AAV central nervous system entry.[34] Fortunately, the C57BL6 lines do express this allele and are susceptible to systemic transduction of the brain by the PHP.eB serotype.

In summary, we suggest this approach provides a convenient model in which to test hypotheses regarding amyloid induction of tauopathy and to screen for agents that might abrogate this induction. Future studies will examine temporal effects of AAV-tau administration on the extent of tauopathy induction, and test agents to suppress this induction as potential therapeutics for AD.

ACKNOWLEDGMENTS

DM serves on the external advisory boards for SynapsDx and Minimmune. DM receives project support from Bright Minds, Danaher, and Hesperos. None of these relationships is related to the topic of this manuscript. The remaining authors have no conflicts to disclose. This work was funded by R01 AG 051500 (to DM), R01 AG 062217 (to MNG), and R01 AG 055072 (to DM).

CONFLICT OF INTEREST STATEMENT

Author disclosures are available in the supporting information.

ORCID

Dylan J. Finneran https://orcid.org/0000-0001-7593-9432
Marcia N. Gordon https://orcid.org/0000-0002-4051-9283

REFERENCES

1. Hardy JA, Higgins GA. Alzheimer's disease: the amyloid cascade hypothesis. *Science*. 1992;256:184-185.
2. Sims JR, Zimmer JA, Evans CD, et al. Donanemab in early symptomatic Alzheimer disease: the TRAILBLAZER-ALZ 2 randomized clinical trial. *JAMA*. 2023;330:512-527.
3. van Dyck CH, Swanson CJ, Aisen P, et al. Lecanemab in early Alzheimer's disease. *N Engl J Med*. 2023;388:9-21.
4. Lewis J, Dickson DW, Lin W-L, et al. Enhanced neurofibrillary degeneration in transgenic mice expressing mutant tau and APP. *Science*. 2001;293:1487-1491.
5. Ribe EM, Perez M, Puig B, et al. Accelerated amyloid deposition, neurofibrillary degeneration and neuronal loss in double mutant APP/tau transgenic mice. *Neurobiol Dis*. 2005;20:814-822.
6. Li T, Braunstein KE, Zhang J, et al. The neuritic plaque facilitates pathological conversion of tau in an Alzheimer's disease mouse model. *Nat Commun*. 2016;7:12082.
7. Pickett EK, Herrmann AG, McQueen J, et al. Amyloid beta and tau cooperate to cause reversible behavioral and transcriptional deficits in a model of Alzheimer's disease. *Cell Rep*. 2019;29:3592-3604 e5.
8. Hurtado DE, Molina-Porcel L, Iba M, et al. Abeta accelerates the spatiotemporal progression of tau pathology and augments tau amyloidosis in an Alzheimer mouse model. *Am J Pathol*. 2010;177:1977-1988.
9. Saito T, Mihira N, Matsuba Y, et al. Humanization of the entire murine Mapt gene provides a murine model of pathological human tau propagation. *J Biol Chem*. 2019;294:12754-12765.
10. Spurrier J, Nicholson L, Fang XT, et al. Reversal of synapse loss in Alzheimer mouse models by targeting mGluR5 to prevent synaptic tagging by C1Q. *Sci Transl Med*. 2022;14:eabi8593.
11. Terwel D, Muyllaert D, Dewachter I, et al. Amyloid activates GSK-3beta to aggravate neuronal tauopathy in bigenic mice. *Am J Pathol*. 2008;172:786-798.
12. Chabrier MA, Cheng D, Castello NA, Green KN, LaFerla FM. Synergistic effects of amyloid-beta and wild-type human tau on dendritic spine loss in a floxed double transgenic model of Alzheimer's disease. *Neurobiol Dis*. 2014;64:107-117.
13. Oddo S, Billings L, Kesslak JP, Cribbs DH, LaFerla FM. Abeta immunotherapy leads to clearance of early, but not late, hyperphosphorylated tau aggregates via the proteasome. *Neuron*. 2004;43:321-332.
14. Bolmont T, Clavaguera F, Meyer-Luehmann M, et al. Induction of tau pathology by intracerebral infusion of amyloid-beta -containing brain extract and by amyloid-beta deposition in APP x Tau transgenic mice. *Am J Pathol*. 2007;171:2012-2020.
15. Gotz J, Chen F, van Dorpe J, Nitsch RM. Formation of neurofibrillary tangles in P301L tau transgenic mice induced by Aß42 fibrils. *Science*. 2001;293:1491-1495.
16. Shen LL, Li WW, Xu YL, et al. Neurotrophin receptor p75 mediates amyloid beta-induced tau pathology. *Neurobiol Dis*. 2019;132:104567.
17. He Z, Guo JL, McBride JD, et al. Amyloid-beta plaques enhance Alzheimer's brain tau-seeded pathologies by facilitating neuritic plaque tau aggregation. *Nat Med*. 2018;24:29-38.
18. Vergara C, Houben S, Suain V, et al. Amyloid-beta pathology enhances pathological fibrillary tau seeding induced by Alzheimer PHF in vivo. *Acta Neuropathol*. 2019;137:397-412.
19. Klein RL, Lin WL, Dickson DW, et al. Rapid neurofibrillary tangle formation after localized gene transfer of mutated tau. *Am J Pathol*. 2004;164:347-353.
20. Sobrido M-J, Miller BL, Havlioglu N, et al. Novel tau polymorphisms, tau haplotypes, and splicing in familial and sporadic frontotemporal dementia. *Arch Neurol*. 2003;60:698-702.
21. Dassie E, Andrews MR, Bensadoun JC, et al. Focal expression of adeno-associated viral-mutant tau induces widespread impairment in an APP mouse model. *Neurobiol Aging*. 2013;34:1355-1368.
22. Koller EJ, Ibanez KR, Vo Q, et al. Combinatorial model of amyloid beta and tau reveals synergy between amyloid deposits and tangle formation. *Neuropathol Appl Neurobiol*. 2022;48:e12779.
23. Chan KY, Jang MJ, Yoo BB, et al. Engineered AAVs for efficient noninvasive gene delivery to the central and peripheral nervous systems. *Nature Neurosci*. 2017;20:1172-1179.
24. Finneran DJ, Njoku IP, Flores-Pazarin D, et al. Toward development of neuron specific transduction after systemic deliver of viral vectors. *Front Neurol*. 2021;12:685802.
25. Holcomb L, Gordon MN, McGowan E, et al. Accelerated Alzheimer-type phenotype in transgenic mice carrying both mutant *amyloid precursor protein* and *presenilin 1* transgenes. *Nat Med*. 1998;4:97-100.

26. Burger C, Nash KR. Small-scale recombinant adeno-associated virus purification. *Methods Mol Biol*. 2016;1382:95-106.
27. Gordon MN, Holcomb LA, Jantzen PT, et al. Time course of the development of Alzheimer-like pathology in the doubly transgenic PS1+APP mouse. *Exp Neurol*. 2002;173:183-195.
28. Paulson JB, Ramsden M, Forster C, Sherman MA, McGowan E, Ashe KH. Amyloid plaque and neurofibrillary tangle pathology in a regulatable mouse model of Alzheimer's disease. *Am J Pathol*. 2008;173:762-772.
29. Thal DR, Rüb U, Orantes M, Braak H. Phases of A beta-deposition in the human brain and its relevance for the development of AD. *Neurology*. 2002;58:1791-1800.
30. Carty N, Lee D, Dickey C, et al. Convection-enhanced delivery and systemic mannitol increase gene product distribution of AAV vectors 5, 8, and 9 and increase gene product in the adult mouse brain. *J Neurosci Methods*. 2010;194:144-153.
31. Mathiesen SN, Lock JL, Schoderboeck L, Abraham WC, Hughes SM. CNS transduction benefits of AAV-PHP.eB over AAV9 are dependent on administration route and mouse strain. *Mol Ther Methods Clin Dev*. 2020;19:447-458.
32. Lippi SLP, Smith ML, Flinn JM. A novel hAPP/htau mouse model of Alzheimer's disease: inclusion of APP with tau exacerbates behavioral deficits and zinc administration heightens tangle pathology. *Front Aging Neurosci*. 2018;10:382.
33. Xu G, Ulm BS, Howard J, et al. TAPPing into the potential of inducible tau/APP transgenic mice. *Neuropathol Appl Neurobiol*. 2022;48:e12791.
34. Huang Q, Chan KY, Tobey IG, et al. Delivering genes across the blood-brain barrier: LY6A, a novel cellular receptor for AAV-PHP.B capsids. *Plos One*. 2019;14:e0225206.

SUPPORTING INFORMATION

Additional supporting information can be found online in the Supporting Information section at the end of this article.

How to cite this article: Finneran DJ, Desjarlais T, Henry A, Jackman BM, Gordon MN, Morgan D. Induction of tauopathy in a mouse model of amyloidosis using intravenous administration of adeno-associated virus vectors expressing human P301L tau. *Alzheimer's Dement*. 2024;10:e12470. https://doi.org/10.1002/trc2.12470